Advances in Science and Technology Research Journal

Advances in Science and Technology Research Journal 2023, 17(4), 110–120
https://doi.org/10.12913/22998624/169343
ISSN 2299-8624, License CC-BY 4.0

Received: 2023.05.11
Accepted: 2023.07.06
Published: 2023.08.12

Experimental and Theoretical Investigation of Galvanized Steel and Fiber-Reinforced Polymer Composites Textile Adhesive Double Lap Joints

Maciej Adam Dybizbański[1*], Katarzyna Rzeszut[2]

[1] Faculty of Civil and Transport Engineering, Poznań University of Technology, ul. Marii Skłodowskiej-Curie 5, 60-965 Poznań, Poland

[2] Faculty of Civil and Transport Engineering, Poznań University of Technology, ul. Marii Skłodowskiej-Curie 5, 60-965 Poznań, Poland

* Corresponding author's e-mail: maciej.dybizbanski@doctorate.put.poznan.pl

ABSTRACT

This paper presents an experimental analysis of fiber-reinforced polymer composites (CFRP) fabric to galvanized steel adhesive connection. An experimental research has been conducted on the adhesive connection between CFRP fabric and galvanized steel subjected to shear forces. The specimens were made from the steel plates overlapped on both sides with SikaWrap 230 C fabric using SikaDur 330 adhesive. Observations of natures of failure for CFRP-steel adhesive connection were conducted based on visual inspection using a scanning microscope. Mixed nature of the connection failure was specified. Moreover, an advanced numerical model has been developed and later on validated and verified on the basis of performed original laboratory tests. Ultimately, final conclusions were drawn based on the advanced numerical model that has been developed, verified and validated using laboratory tests results, as well as analytical models and nature of the connection failure was specified.

Keywords: cohesive zone model, double lap joint, shear stresses, FEM.

INTRODUCTION

It has been proven that the bonding of fiber reinforced polymer (FRP) composites is a successful method for enhancing the stiffness and strength of structures [1–3]. Due to their benefits, such as their light weight, high specific strength and stiffness, great durability performances, exceptional fatigue and corrosion resistance, and ease of assembly, FRP materials have gained growing interest in the strengthening steel structures. FRPs are therefore very promising for structural repair and strengthening and, in many situations, far superior to traditional steel plates [1–9].

Although substantial study has been done on FRP strengthened concrete [10–14], CFRP-to-steel bonded interactions have received less attention [1, 15]. The concrete acts as the weakest link in the FRP to concrete bond. However, there are numerous ways that the FRP-to-steel connection could be weak [16]. Failure modes examples for CFRP-Steel adhesive connection can be described as: adhesion failure at the CFRP/adhesive interface (1), adhesion failure at the steel/adhesive interface (2), cohesive failure in the adhesive (3), CFRP delamination (4) and CFRP rupture (5).

As mentioned, a material might fail in a way called delamination in which it separates into layers. In example, shear stresses and loads applied perpendicular to the high strength layers in FRP composites can result in the fracture of the polymer matrix or the debonding of the fiber reinforcement from the polymer [17].

Bonding strength is a product of both chemical and mechanical bonding between the two adherents [18]. Failure modes (1) and (2) together

are referred to as adhesion interface failure, hence they are considered as chemical failures. Since either the adhesive or the CFRP breaks in failure modes (3), (4) and (5), they are referred to as material failures. The material qualities in this situation determine the bonding strength. If the failure mode is adhesive interface failure, the adhesion strength, which mostly depends on the surface treatment of the FRP or steel, controls the effectiveness of the FRP-strengthened steel structures.

The design theory must focus more on the characteristics of the adhesive and CFRP laminates if the failure mode is material failure. Different failure mechanisms are correlated with certain design factors.

So far, to the best knowledge of the authors, no research has been conducted on galvanized steel bonded with carbon fiber textile. Most of the studies involve tests on CFRP tapes and raw steel. In addition, the results presented in this article are part of a larger research activity to determine the effectiveness of strengthening Thin-Walled Cold-Formed Steel (TWCFS) sigma beams with bonded CFRP textiles. For this reason, the aim is also to determine the adhesive steel-CFRP connection parameters for an advanced numerical model. Henceforth, an experimental research has been conducted on the commonly known adhesive Double Lap Joints (DLJ) [19–22] between carbon fibre textile and galvanized steel subjected to shear forces. The shear strength of the adhesive was determined based on original testing method due to the lack of standard guidelines for the connection and materials under consideration. Therefore, the authors decided that they would propose a test element that would relate to standard material tests on steel with the difference that the steel specimen is split in half lengthwise.

The research activity was started by conducting experimental laboratory tests on adhesive connection subjected to shear forces. Subsequently, examination of damaged samples was conducted, followed by development of the numerical model and analytical analysis. Ultimately, the comparative analysis between laboratory, numerical and analytical tests was performed. Figure 1 shows the flowchart of the analysis process.

EXPERIMENTAL TESTS

The bonding length of the textile is derived from the maximum length of the available bonding area minus 5 mm due to possible imperfections in the fabrication of the specimen. The width of 20 mm is the same as in [23]. The specimens were made from steel plates overlapped on both sides with SikaWrap 230 C [24] matting using SikaDur 330 [25] adhesive. SikaWrap 230 C is a woven unidirectional carbon fibre fabric and SikaDur 330 is a 2-component, thixotropic epoxy based impregnating resin and adhesive. The tests were carried out on 5 specimens. Overlap length of 55 mm and adhesive thickness of 0.5 mm was considered. The samples were made as shown in Figure 2. Before creating bonding connection, the steel plates' thicknesses were measured. The steel plate surface was cleaned with sandpaper and degreased with acetone. After surface preparation the adhesive layer was applied uniformly on the steel plate surface, followed by one layup of CFRP textile. The CFRP textile was pressed to the steel surface creating a bonded connection and embedding the CFRP fibers in epoxy matrix. Moreover, the excess of adhesive has been removed from the surface of the textile. After the hardening process of the adhesive was finished, which took 7 days, the measurement of thickness of the connection has been performed. The difference between second and first measurement, reduced by CFRP textile thickness of 0.129 mm, was the adhesive thickness.

For experimental testing INSTRON SATEC 300 DX testing machine was used. Load accuracy measurement was 0.6 kN and displacement

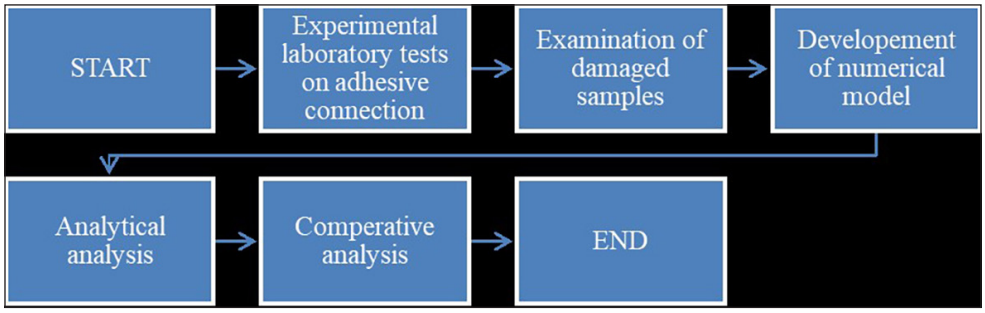

Fig. 1. The flowchart of analysis process

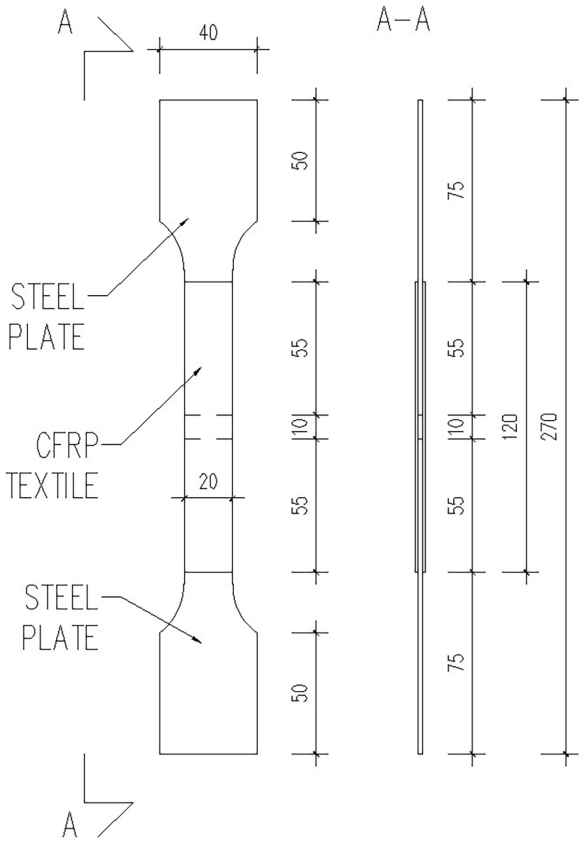

Fig. 2. Schematic of the sample

accuracy was 0.13 mm. The testing machine was set to zero after the test loading system was assembled, but before the specimen was actually gripped at both ends. Once the force zero point was set, the force measurement system was not altered in any way during the test. The positioning of the specimen in the jaws of the testing machine was such that no bending loads were induced. The shear tests were carried out under displacement control conditions. The samples were stretched at the speed of 0.05 mm/s until the specimens failed.

Fig. 3. First series samples – shear strength

Fig. 4. Test stand - SK1 series specimen in the grips of a testing machine

The prepared specimens are shown in Figure 3. The adhesive shear test stand is shown in Figure 4.

After completion of the laboratory tests, observations of natures of fracture for CFRP-Steel adhesive connection were conducted. Visual inspection was carried out, as well as, the images of the samples were taken using a scanning microscope.

NUMERICAL ANALYSIS

Coupled cohesive zone models use mixed-mode cohesive laws to take into account the interaction between mode I loading and mode II to loading [26]. In contrast, uncoupled cohesive zone models that assume the cohesive laws in the normal direction and the tangential (shear) direction are independent of one another [27, 28]. The fracture energy in mode II loading is frequently substantially bigger than that in mode I loading, according to comprehensive experimental evidence. However, several mixed-modal cohesive laws presume that the fracture energy is the same for both loading modes [29, 30]. The fracture energy for shear loading mode is inspected in the current work.

The cohesive law used in the current work takes into account shear stresses and deformations, namely those along the interface. Bond stresses are referred to jointly as tractions, whilst interfacial deformations are referred to collectively as separations. The normal traction and the two shear tractions, which are represented by t_n, t_s, and t_t, respectively, make up the three components of the traction vector. The relevant separations are similarly indicated by δ_n, δ_s, and δ_t,

respectively. After describing initial thickness as T_a, it is simple to write:

$$\varepsilon_{\mathrm{n}} = \frac{\delta_n}{T_a};\ \varepsilon_s = \frac{\delta_s}{T_a};\ \varepsilon_{\mathrm{t}} = \frac{\delta_t}{T_a} \tag{1}$$

where: ε_n, ε_s, and ε_t – strains in the normal and the two shear directions respectively.

The interfacial behaviour before damage initiation can thus be represented by:

$$\begin{Bmatrix} t_n \\ t_s \\ t_t \end{Bmatrix} = \begin{bmatrix} K_{nn} & 0 & 0 \\ 0 & K_{ss} & 0 \\ 0 & 0 & K_{tt} \end{bmatrix} \begin{Bmatrix} \delta_n \\ \delta_s \\ \delta_t \end{Bmatrix} \tag{2}$$

where: K_{nn}, K_{ss}, and K_{tt} – the elastic stiffnesses in the normal and the two shear directions respectively.
K_{nn} is equal to the initial slope of the traction-separation model for mode I [31] and can be described as:

$$\mathrm{K_{nn}} = \frac{E_a}{T_a} \tag{3}$$

where: E_a – tensile elastic modulus of an adhesive;
T_a – thickness of the adhesive.

Both K_{ss} and K_{tt} are the same, and are equal to the initial slope of traction-separation model for mode II loading [32] and can be described as:

$$\mathrm{K_{ss}} = K_{tt} = \frac{G_a}{T_a} \tag{4}$$

where: G_a – shear modulus of an adhesive;
T_a – thickness of the adhesive.

For damage initiation criterion, the quadratic nominal stress criterion was adopted. It can be described as:

$$\left\{\frac{\langle t_n \rangle}{t_n^o}\right\}^2 + \left\{\frac{t_s}{t_n^o}\right\}^2 + \left\{\frac{t_t}{t_n^o}\right\}^2 = 1 \tag{5}$$

For predicting interfacial fracture energy (IFE), the equation presented by [33] was adopted. It can be described as:

$$\mathrm{G}_f = 62\left(\frac{\sigma_{max}}{G_a}\right)^{0,56} T_a^{0,27} \tag{6}$$

where: G_a – shear modulus of an adhesive;
T_a – thickness of the adhesive;
σ_{max} – tensile strength / peak bond normal stress.

Furthermore, CFRP fabric material properties were originally taken from [34]. However, many of the original parameters had to be calibrated during verification and validation of the numerical model. Table 1 and 2 presents implemented CFRP and steel properties in FEM respectively.

The coupled Cohesive Zone Model (CZM) was implemented in the commercial FE program ABAQUS [35]. Due to the very low thickness of the adhesive, its impact has been neglected. The cohesive surface was adopted and its constitutive behaviour was defined by the independent mode cohesive law. The cohesive behaviour was defined by creating traction-separation behaviour with coupled and specified stiffness coefficients. The damage initiation behaviour was defined using quadratic traction criterion. The damage

Table 1. CFRP properties implemented in FEM

Parameter	Quantity	Unit
Density	1.83e-9	t/mm^3
Elastic modulus of fabric E1	220000	MPa
Elastic modulus of fabric E2	15750	MPa
Longitudinal and transverse Poisson's ratio	0.3	[-]
Shear modulus G12	8730	MPa
Shear modulus G13	11650	MPa
Shear modulus G23	5615	MPa

Table 2. Steel properties implemented in FEM

Parameter	Quantity	Unit
Density	7.85e-9	t/mm^3
Elastic modulus E	200000	MPa
Longitudinal and transverse Poisson's ratio	0.3	[-]

Table 3. Cohesive surface properties implemented in FEM model

Parameter	Quantity	Unit
Maximum nominal stress in all directions	30	MPa
Fracture energy	6.5	N/mm

evolution behaviour was defined as energy type with exponential softening behaviour. The initial stiffness matrix can be described as:

$$K = \begin{bmatrix} K_{nn} & 0 & 0 \\ 0 & K_{ss} & 0 \\ 0 & 0 & K_{tt} \end{bmatrix} = \begin{bmatrix} 9000 & 0 & 0 \\ 0 & 3460 & 0 \\ 0 & 0 & 3460 \end{bmatrix} \quad (7)$$

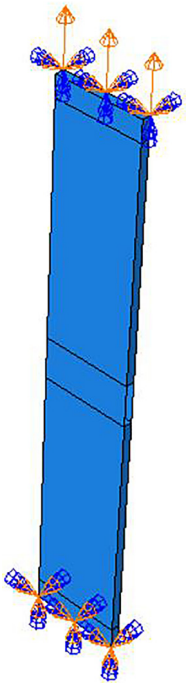

Fig. 5. Applied boundary conditions

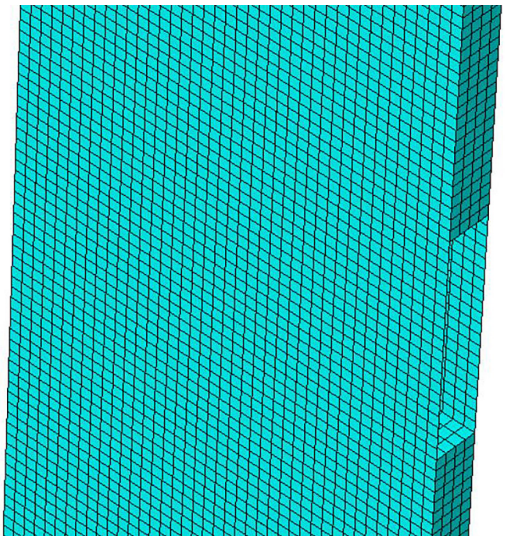

Fig. 6. Applied mesh distribution

The damage properties of cohesive surface are presented in Table 3.

The calculations were conducted using static general procedure accounting geometrical non-linearity and automatic stabilization using dissipated energy fraction of 0.0002. The direct sparse solver was implemented and for solving nonlinear equilibrium equations Newton's method was used.

The boundary conditions applied are presented in Figure 5. On bottom surface the displacements and rotations were all blocked. Similarly, on top surface displacements and rotations were blocked except the vertical displacement which was set to 1.4 mm upwards in order to enforce tension.

For CFRP textile the linear quadrilateral elements of type S4R and for steel plates the linear hexahedral elements of type C3D8R were used. The size of FE mesh was set to 0.5 mm and consisted of 57600 elements and 69372 nodes. The part of mesh distribution is presented in Figure 6.

ANALYTICAL APPROACH

The problem presented can be formulated using the de Bruyne model and the Volkersen model, among others.

De Bruyne's model

One analytical approach for an adhesive DLJ is presented in the works [36–39]. This approach assumes that:

- the adhesive and the adherents behave as linearly elastic bodies;
- the bonded elements are subjected to uniform tension in all sections;
- the eccentricity of the load, which causes bending of the bonded elements, has no effect on the distribution of shear stresses in the adhesive joint;
- the elastic deformation of the bonded components is taken into account.

This model can be represented by equations 8–14.

$$\tau_c(x) = A * \sinh(\beta x) + B * \cosh(\beta x) \quad (8)$$

$$A = \frac{\beta c \tau_{avg}}{\cosh(\beta c)} \left[\frac{1 - \frac{E_2 t_2}{2E_1 t_1}}{1 + \frac{E_2 t_2}{2E_1 t_1}} \right] \quad (9)$$

$$B = \frac{\beta c \tau_{avg}}{\sinh(\beta c)} \quad (10)$$

$$\beta = \alpha^2 \lambda^2 \quad (11)$$

$$\alpha^2 = \frac{1}{\left[1 + \frac{G_a}{T_a}\left(\frac{t_2}{6G_2} + \frac{t_1}{3G_1}\right)\right]} \quad (12)$$

$$\lambda^2 = \frac{G_a}{T_a}\left(\frac{2}{E_2 t_2} + \frac{1}{E_1 t_1}\right) \quad (13)$$

$$\tau_{avg} = \frac{T}{4cw} \quad (14)$$

where: E_1, E_2, G_1, G_2, t_1, t_2 – Young's modulus, Kirchoffs's modulus and thicknesses of adherents;
G_a, T_a – Young's modulus and thicknes of the adhesive;
$L_0 = 2c$ – overlap length;
τ_{avg} – average shear stress in the adhesive layer;
T – tensile force;
w – width of adhesive joint.

Modified Volkersen's model for DLJ

Another approach that can be applied to the presented problem may be Volkersen's elastic model [39]. This model is commonly used for Single Lap Joints (SLJ), despite the fact that it does not account for the bending moment caused by load eccentricity in SLJ. The authors of [40] presented a modified version of Volkersen's model, which was extended for DLJ. This model can be formulated as:

$$\tau = \frac{P}{bL_0}\frac{w}{2}\frac{\cosh(wX)}{\sinh\left(\frac{w}{2}\right)} + \\ + \left(\frac{t_1 - t_2}{t_1 + t_2}\right)\frac{w}{2}\frac{\sinh(wX)}{\cosh\left(\frac{w}{2}\right)} \quad (15)$$

where: τ – shear stress in the adhesive;
P – applied load;
b – joint width;
L_0 – overlap length;
t_1, t_2 –adherend's thicknesses.

Additionally, $X = x/L_0$ with $-0.5 \leq X \leq 0.5$. The characteristic shear-lag distance, w, [41] is given by:

$$w = \sqrt{\frac{l^2}{Et_1 t_a}\left(1 + \frac{t_1}{t_2}\right)} \quad (16)$$

where: G – adhesive shear modulus;
E – adherend elastic modulus;
t_a – adhesive thickness.

RESULTS

Experimental tests results

The test results for the first and second series of specimens are summarised in Table 1. The mean value of: the maximum load and the corresponding imposed displacement was reported for the respective series of specimens. The standard deviation was determined for each parameter. Diagrams of the force-displacement relationship for the test specimens are shown in Figure 7.

The initial slow increase in force due to the initial imperfections of the samples can be observed on the graph. Once a displacement of approximately 1.1 mm is reached, there is a sudden

Table 4. Adhesive shear strength test results for the first series

No.	Sample label	Maximum load (kN)	Displacement at maximum load (mm)
1	SK1.1	6.806	2.765
2	SK1.2	9.475	2.629
3	SK1.3	8.953	2.740
4	SK1.4	7.600	2.228
5	SK1.5	7.929	2.218
Average		8.153	2.516
Standard deviation		1.06755	0.27230

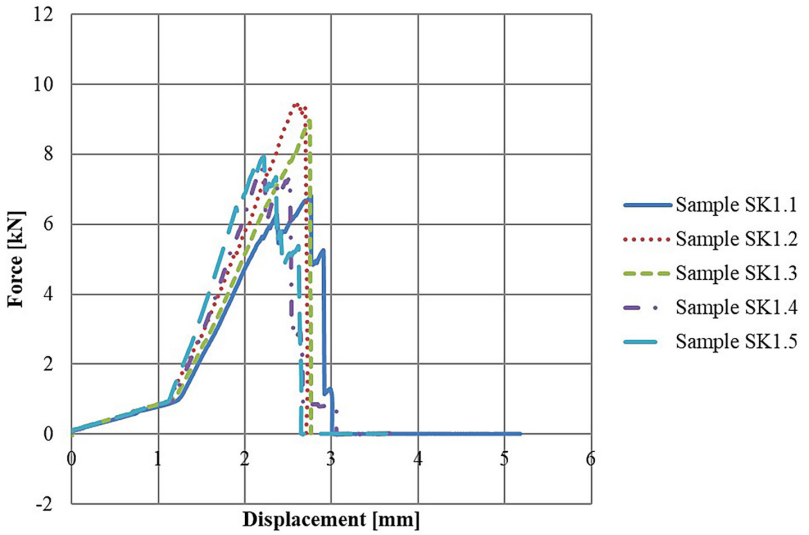

Fig. 7. Force – displacement diagram for the test series

increase in force which is a straight line until the specimen breaks. The destruction of the joint occurs gradually, with successive fragments of CFRP textile breaking off of the steel surface. The maximum, minimum and average rupture force values are 9.475 kN, 6.806 kN and 8.153 kN respectively.

Observation of connection structure damage

Observations of natures of fracture for CFRP-Steel adhesive connection were conducted. Visual inspection was carried out, as well as, the images of the samples were taken using a scanning microscope. Figure 8 shows damaged samples.

Upon visual inspection of the damaged samples, different types of damage were observed. On sample SK1.3 damage was observed at the steel/adhesive interface, but only on the part of the surface. Some of the fibers were still bonded to the surface. However, samples SK1.1, SK1.2 and SK1.5 represent debonding on whole surface at steel/adhesive interface. Ultimately, sample SK1.4 was the only one where CFRP delamination was noted among partial debonding at steel/adhesive interface. After the inspection was finished, sample SK1.1 undergo further investigation using scanning microscope. The results are presented on Figures 9 and 10.

Fig. 8. Damaged first series samples – shear strength

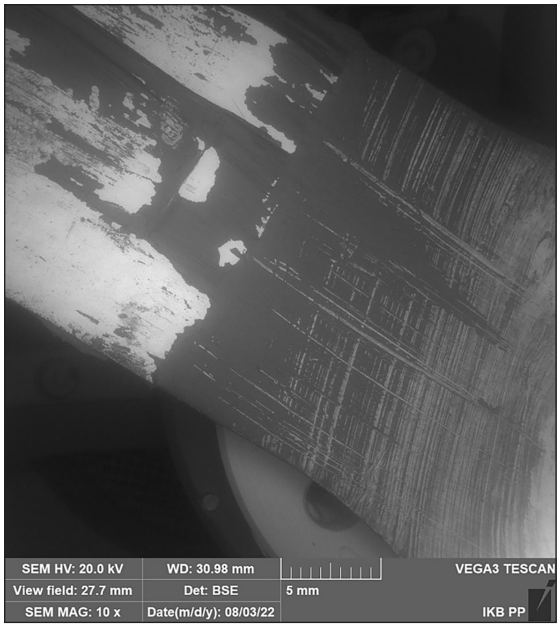

Fig. 9. Damaged SK1.1 sample – steel paddle

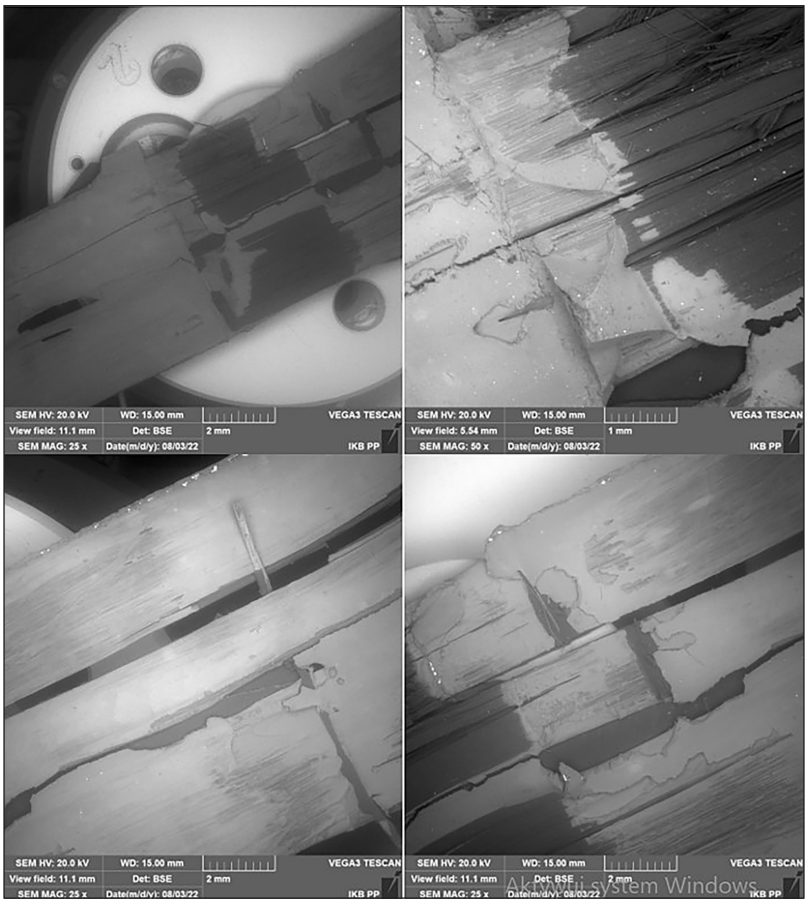

Fig. 10. Damaged SK1.1 sample – FRP fabric

On the other hand Figure 8 presents the surface of the steel sample after debonding. It can now be observed that thin layers of adhesive remain in some areas. However, the initial observations can be confirmed. Mainly the failure occurred at the steel/adhesive interface, accompanied by cohesive failure in the adhesive layer.

Considering presented on Figure 11 zoomed surface of debonded CFRP fabric, its state indicates that failure occurred at the steel/adhesive interface. Most of the surface is still covered in the adhesive, with only small spots without it. It can be once again confirmed, that the failure occurred at the steel/adhesive interface, accompanied by

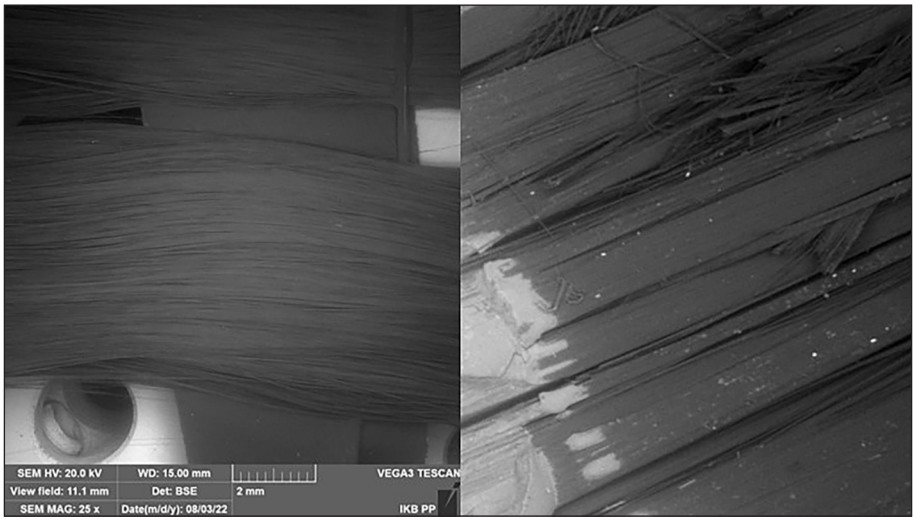

Fig. 11. Undamaged and damaged CFRP fabric

cohesive failure in the adhesive layer. It can be stated that the nature of failure for presented sample is of mixed character. In addition to these observations, after analysis of images from the scanning microscope, damage of the CFRP fabric fibres was noted. Figure 10 presents magnified undamaged and damaged CFRP fabric.

After analysis of nature of fracture for considered CFRP-Steel adhesive connection, it can be noted that the most common failure in all samples happened at the steel/adhesive interface. Furthermore, in several small places the cohesive failure in the adhesive was observed, as well as, CFRP delamination.

Verification and validation of numerical model

Figure 12 presents the results of numerical analysis in comparison to average values obtained from laboratory tests for SK1 samples. It can be noted that the numerical model reflects well the actual samples behaviour obtained during laboratory tests in the range from the start of loading to the plateau in the force-displacement diagram.

Unfortunately, after reaching the limit point, the numerical calculations break down due to the lack of convergence of the numerical solution. In addition, in the range of displacements from 0 to 1 mm, a discrepancy between the laboratory and numerical test results can also be noticed. This is due to the fact that the CFRP fabric start to contributed in bearing capacity when it is in the tensile stress range. In laboratory tests, in the initial phase of work, due to insufficient stretching of the fabric, zero load capacity of the connection can be noticed. Summing up, the proposed numerical model of the adhesive joint well describes laboratory tests in the range of tensile stresses until reaching the limit point. However, in the scope after passing the limit point, it requires further corrections and improvements.

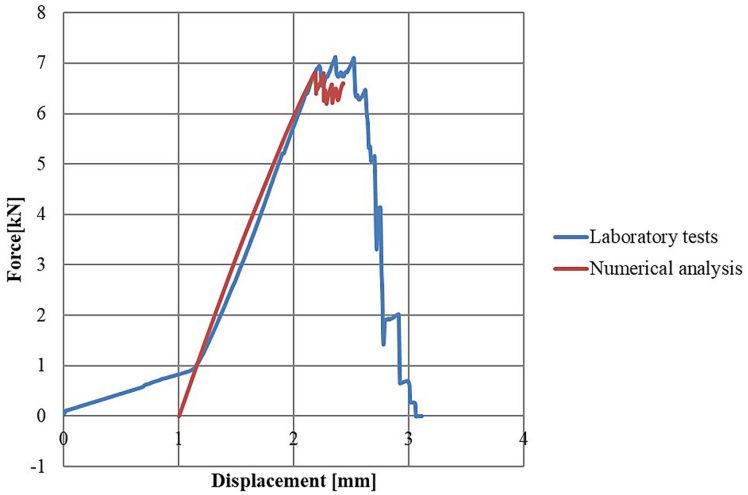

Fig. 12. Force-displacement diagrams

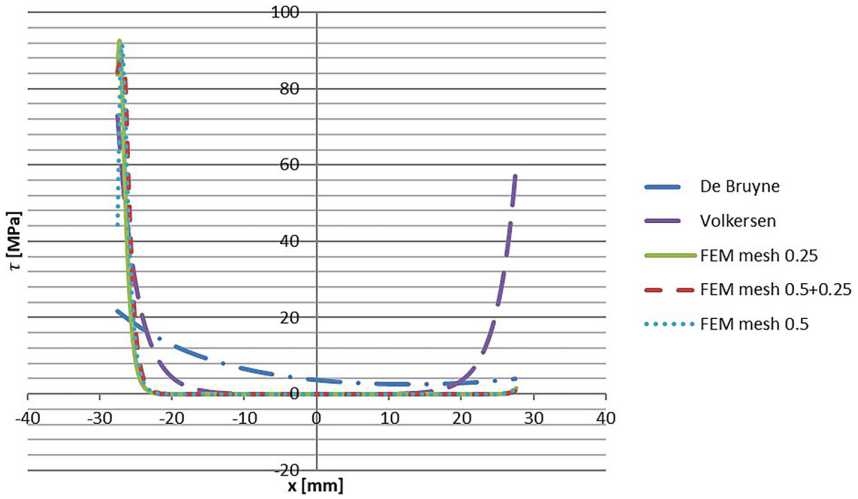

Fig. 13. Shear stresses along the joint's length

Stress analysis

Using the analytical models presented, as well as the numerical model, it is possible to describe the shear stress values along the length of the joint (Fig. 13). All graphs were presented for maximum tensile force value of 7 kN. It can be noted that different mesh density has no impact on the results from the numerical model, therefore the conclusion that the numerical model is reliable. Moreover, it aligns well with the modified Volkersen's analytical model. Although, it can be observed that de Bruyne's model differ significantly, henceforth cannot be used for prediction of presented joint's strength.

CONCLUSIONS

The article presents an experimental analysis of CFRP fabric to galvanized steel adhesive connection. The original lab study was carried out on 5 test specimens. Samples were double-lap CFRP-steel adhesive joints subjected to shear forces. Moreover the advanced numerical model has been developed, verified and validated using laboratory tests results, as well as analytical models. Complex nature of the connection failure was specified. Failure occurred at the steel/adhesive interface, accompanied by cohesive failure in the adhesive layer, CFRP delamination and rupture of CFRP textile fibres.

Additional conclusions based on FEM and analytical analyses were drawn. Equation (6) is not fully suitable for predicting interfacial fracture energy for tested samples. Stiffness of the adhesive has no significant impact on presented force-displacement relation. The initial inclination of the force-displacement curve is mainly determined by the strength characteristic of the CFRP fabric. For linear-exponential Cohesive Zone Model (CZM) the initial slope of force-displacement curve tends to be closer to straight line in comparison to bilinear CZM. Volkersen's model is suitable to be used for prediction of traction for presented joint. De Bruyne's model may provide undervalued results for presented joint. The presented numerical model of adhesive DLJ has the potential to be used for development of strengthened with CFRP textiles TWCFS beams.

Acknowledgements

This paper was financially supported by Poznan University of Technology: 0412/SBAD/0070, 0412/SBAD/0071.

REFERENCES

1. Zhao X., Zhang L. State-of-the-art review on FRP strengthened steel structures. Engineering Structures. 2007; 29(8): 1808–1823.
2. Gholami M., Sam A., Yatim J., Tahir M. A review on steel/CFRP strengthening systems focusing environmental performance. Construction and Building Materials. 2013; 47: 301–310.
3. Tafsirojjaman T., Ur Rahman Dogar A., Liu Y., Manalo A., Thambiratnam D.P. Performance and design of Steel Structures Reinforced with FRP Composites: A state-of-the-art review. Engineering Failure Analysis. 2022; 138: 106371. DOI: 10.1016/j.engfailanal.2022.106371
4. Bambach M., Elchalakani M. Plastic mechanism analysis of steel SHS strengthened with CFRP under large axial deformation. Thin-Walled Structures. 2007; 45(2): 159–170.
5. Bambach M., Jama H., Elchalakani M. Axial capacity and design of thin-walled steel SHS strengthened with CFRP. Thin-Walled Structures. 2009; 47(10): 1112–1121.
6. Bambach M. Numerical simulation of the shock spalling failure of bonded fibre–epoxy strengthening systems for metallic structures. Engineering Structures. 2014; 64: 1–11.
7. Szewczak I., Rzeszut K., Rozylo P., Samborski S. Laboratory and Numerical Analysis of Steel Cold-Formed Sigma Beams Retrofitted by Bonded CFRP Tapes. Materials. 2020; 13(19): 4339.
8. Szewczak I., Rozylo P., Rzeszut K. Influence of Mechanical Properties of Steel and CFRP Tapes on the Effectiveness of Strengthening Thin-Walled Beams. Materials. 2021; 14(9): 2388.
9. Tafsirojjaman T., Fawzia S., Thambiratnam D., Zhao X. FRP strengthened SHS beam-column connection under monotonic and large-deformation cyclic loading. Thin-Walled Structures. 2021; 161: 107518.
10. Sanginabadi K., Mostofinejad D. Effect of aggregate content on the CFRP-concrete effective bond length: An experimental and analytical study. Composite Structures. 2021; 269: 114044.
11. Yun Y., Wu Y. Durability of CFRP–concrete joints under freeze–thaw cycling. Cold Regions Science and Technology. 2011; 65(3): 401–412.
12. Zhang W., Tang Z. Numerical Modeling of Response of CFRP–Concrete Interfaces Subjected to

Fatigue Loading. Journal of Composites for Construction. 2021; 25(5).

13. Zaki M., Rasheed H., Alkhrdaji T. Performance of CFRP-strengthened concrete beams fastened with distributed CFRP dowel and fiber anchors. Composites Part B: Engineering. 2019; 176: 107117.
14. Li G., Tan K., Fung T. Experimental study on CFRP-concrete dynamic debonding behaviour. Engineering Structures. 2020; 206: 110055.
15. Teng J., Yu T., Fernando D. Strengthening of steel structures with fiber-reinforced polymer composites. Journal of Constructional Steel Research. 2012; 78: 131–143.
16. ISO 4624:2016 – Paints and varnishes – Pull-off test for adhesion
17. Cantwell W.J., Morton J. The impact resistance of composite materials – A review. Composites. 1991; 22(5): 347–62. DOI: 10.1016/0010-4361(91)90549-v
18. Ren H., Chen X., Chen Y. Aircraft reliability and maintainability analysis and design. In: Reliability Based Aircraft Maintenance Optimization and Applications. Elsevier. 2017; 37–78.
19. da Silva L.F.M., das Neves P.J.C., Adams R.D., Spelt J.K. Analytical models of adhesively bonded joints – part I: Literature survey. International Journal of Adhesion and Adhesives. 2009; 29(3): 319–30. DOI: 10.1016/j.ijadhadh.2008.06.005
20. Marchione F. Stress distribution in double-lap adhesive joints: Effect of adherend reinforcement layer. International Journal of Adhesion and Adhesives. 2021; 105: 102780. doi:10.1016/j.ijadhadh.2020.102780
21. Shin K.C., Lee J.J. Bond parameters affecting failure of co-cured single and double lap joints subjected to static and dynamic tensile loads. European Structural Integrity Society. 2003; 373–84. DOI: 10.1016/s1566-1369(03)80110-3
22. Hou X., Yousefi Kanani A., Ye J. Double lap adhesive joint with reduced stress concentration: Effect of slot. Composite Structures. 2018; 202: 635–42. DOI: 10.1016/j.compstruct.2018.03.026
23. EN ISO 6892-1:2020 – Metallic materials - Tensile testing - Part 1: Method of test at room temperature
24. [Internet]. Gcc.sika.com. 2022 [cited 3 September 2022]. Available from: https://gcc.sika.com/content/dam/dms/gcc/j/sikawrap_-230_c.pdf
25. [Internet]. Usa.sika.com. 2022 [cited 3 September 2022]. Available from: https://usa.sika.com/content/dam/dms/us01/0/sikadur_-330.pdf
26. De Lorenzis L., Fernando D., Teng J.-G. Coupled mixed-mode cohesive zone modeling of interfacial debonding in simply supported plated beams. International Journal of Solids and Structures. 2013; 50(14-15): 2477–94.
27. de Morais A.B. Mode I cohesive zone model for delamination in composite beams. Engineering Fracture Mechanics. 2013; 109: 236–45.
28. Monteiro J., Akhavan-Safar A., Carbas R., Marques E., Goyal R., El-zein M., et al. Mode II modeling of adhesive materials degraded by fatigue loading using cohesive zone elements. Theoretical and Applied Fracture Mechanics. 2019; 103: 102253.
29. Högberg J. Mixed mode cohesive law. International Journal of Fracture. 2006; 141(3–4): 549–559.
30. Benamar B., Mokhtari M., Madani K., Benzaama H. Using a cohesive zone modeling to predict the compressive and tensile behavior on the failure load of single lap bonded joint. Frattura ed Integrità Strutturale. 2019; 19; 13(50): 112–25.
31. Turon A., Dávila C.G., Camanho P.P., Costa J. An engineering solution for mesh size effects in the simulation of delamination using cohesive zone models. Engineering Fracture Mechanics. 2007; 74(10): 1665–82.
32. Teng J.G., Fernando D., Yu T. Finite element modelling of debonding failures in steel beams flexurally strengthened with CFRP laminates. Engineering Structures. 2015; 86: 213–24.
33. Xia S., Teng J. Behaviour of FRP-to-Steel Bonded joints. International Symposium on Bond Behaviour of FRP in Structures (BBFS 2005). 2005. Hong Kong. China, 419–426.
34. Raza A., Khan Q. uz Z., Ahmad A. Prediction of Axial Compressive Strength for FRP-Confined Concrete Compression Members. KSCE Journal of Civil Engineering. 2020; 24(7): 2099–109.
35. Abaqus Unified FEA [Internet]. 3ds.com. [cited 2022 Nov 22]. Available from: https://www.3ds.com/products-services/simulia/products/abaqus/
36. de Bruyne NA. The strength of glued joints. Aircraft Engineering and Aerospace Technology. 1944; 16(4): 115–8.
37. Oplinger D.W. Effects of adherend deflections in single lap joints. International Journal of Solids and Structures. 1994; 31(18): 2565–87.
38. Tsai M.Y., Oplinger D.W., Morton J. Improved theoretical solutions for adhesive lap joints. International Journal of Solids and Structures. 1998; 35(12): 1163–85.
39. Volkersen O. Die Niektraftverteilung in Zugbeanspruchten mit Konstanten Laschenquerschritten. Luftfahrtforschung. 1938; 15: 41–47.
40. Gonçalves D.C., Sánchez-Arce I.J., Ramalho L.D., Campilho R.D., Belinha J. Introductory application of a natural neighbour meshless elastic formulation to double-lap adhesive joints. Journal of the Brazilian Society of Mechanical Sciences and Engineering. 2022; 44(2).
41. Quispe Rodríguez R., de Paiva W.P., Sollero P., Bertoni Rodrigues M.R., de Albuquerque É.L. Failure criteria for adhesively bonded joints. International Journal of Adhesion and Adhesives. 2012; 37: 26–36.